

Deep S³PR: Simultaneous Source Separation and Phase Retrieval Using Deep Generative Models

Christopher A. Metzler¹ Gordon Wetzstein¹

Abstract

This paper introduces and solves the simultaneous source separation and phase retrieval (S³PR) problem. S³PR shows up in a number application domains, most notably computational optics, where one has multiple independent coherent sources whose phase is difficult to measure. In general, S³PR is highly under-determined, non-convex, and difficult to solve. In this work, we demonstrate that by restricting the solutions to lie in the range of a deep generative model, we can constrain the search space sufficiently to solve S³PR.

1. Introduction

We define the S³PR problem as follows. Recover the signals $x_1, x_2, \dots, x_L \in \mathcal{C}$, where \mathcal{C} is some subset of \mathbb{R}^n (e.g. the set of natural images), from a noisy measurement vector $y \in \mathbb{R}^m$ given by

$$y = \sum_{l=1}^L |\mathbf{A}_l x_l|^2 + w, \quad (1)$$

where the square is elementwise, the measurement matrices $\mathbf{A}_l \in \mathbb{C}^{m \times n}$ are known for all l , and w represents additive noise. In the remainder, we focus on the special case $\mathbf{A}_1 = \mathbf{A}_2 = \dots = \mathbf{A}_L$.

For $L = 1$ this problem is just standard phase retrieval (PR), a problem for which myriad solutions exist (Gerchberg, 1972; Fienup, 1978; 1982; Griffin & Lim, 1984). However, when $L > 1$ things become significantly more challenging. In particular, one is forced to disentangle the components of y that came from x_i from the components that came from x_j , with $i \neq j$. That is one must solve a source separation (SS) problem as well.

Motivation S³PR shows up in a variety of different application domains whenever one measures the intensity of

¹Department of Electrical Engineering, Stanford University, California, USA. Correspondence to: Christopher A. Metzler <cmetzler@stanford.edu>.

a field formed by multiple independent coherent sources. Under these conditions, the fields within a source add but the intensities between sources add. This situation appears in X-ray coherent diffraction imaging with multiple sources (Miao et al., 1999), correlation-based imaging through thin scattering media and around corners with highly separated objects (Bertolotti et al., 2012; Katz et al., 2014; Metzler et al., 2020), transmission-matrix based imaging through thick scattering media with multiple independent sources (Rajaei et al., 2016; Sharma et al., 2019), and even multiple source localization with mmWave 5G (Hasanah et al., 2018).

Despite the prevalence of the S³PR problem, we are unaware of any existing S³PR solutions. The lack of existing solutions is likely because S³PR is simply too non-convex and under-determined to be solved with conventional algorithms. While a cascaded solution, that is SS followed by PR, could work in principle, in practice the components $|\mathbf{A}x_1|^2, |\mathbf{A}x_2|^2, \dots, |\mathbf{A}x_L|^2$ are too similar to separate with existing SS algorithms.

Our contribution In this work we solve the S³PR problem by imposing strong but realistic priors on the reconstructed signals. In particular, we constrain x_1, x_2, \dots, x_L to lie in the range of a generative neural network $G: \mathbb{R}^k \rightarrow \mathbb{R}^n$ with $k \ll n$. That is, $\mathcal{C} = \text{Range}(G)$ and for all $x_l \in \mathcal{C}$ there exists some latent vector $z_l \in \mathbb{R}^k$ such that $x_l = G(z_l)$.

Using this constraint, we recover x_1, x_2, \dots, x_L , with our estimates $\hat{x}_l = G(\hat{z}_l)$, from y by solving the optimization problem

$$\hat{z}_1, \hat{z}_2, \dots, \hat{z}_L = \arg \min_{z_1, z_2, \dots, z_L} \left\| y - \sum_{l=1}^L |\mathbf{A}G(z_l)|^2 \right\|_2^2, \quad (2)$$

using an alternating descent algorithm.

To our knowledge, this work represents the first solution to S³PR. Accordingly, it opens up a variety of application domains. In Section 5 we apply this method to simulated Gaussian, coded-diffraction-pattern, and Fourier measurements and demonstrate the successful recovery of numbers ($\mathcal{C} = \text{MNIST dataset}$) and articles of clothing ($\mathcal{C} = \text{Fashion MNIST dataset}$ (Xiao et al., 2017)).

Limitations Our results have a few limitations. First, our present reconstructions are low resolution and come from fairly restrictive classes — just digits and articles of clothing. While color datasets like CelebA (Liu et al., 2015) are often also used in the context of solving inverse problems with deep generative models, we chose not to include them here: color images have little practical relevance in the real-world applications where S³PR appears. Secondly, while we provide extensive evidence that deep generative models can be used to solve S³PR, our current results are purely empirical. S³PR remains a highly under-determined and non-convex problem and deriving the conditions under which it can and cannot be solved remains an important but open problem.

2. Related Work

While the S³PR problem is new, both PR and SS have been studied extensively and have a vast literature. Likewise, while not previously used for S³PR, deep generative models have recently been applied to a range of imaging inverse problems. We now highlight a few of the most prominent of these works.

2.1. Phase Retrieval

The optics community has studied the PR problem continuously since the 1970s (Gerchberg, 1972; Fienup, 1978; 1982; Griffin & Lim, 1984; Pfeifer et al., 2006; Rodriguez et al., 2013). In the last decade, PR has caught the attention of the optimization community as well (Candes et al., 2013; 2015a; Goldstein & Studer, 2016; Bahmani & Romberg, 2017). For a benchmark study of over a dozen popular PR algorithms, see PhasePack (Chandra et al., 2017). No existing PR algorithm can handle S³PR.

Compressive phase retrieval (Moravec et al., 2007) recognized that if one imposed a prior on the reconstruction one could perform PR using significantly fewer measurements. This initial work has been followed up by numerous others that have imposed more and more elaborate priors on the reconstruction (Mukherjee & Seelamantula, 2012; Schniter & Rangan, 2015; Tillmann et al., 2016; Metzler et al., 2016). Again, none of these algorithms can handle S³PR.

Multi-source phase retrieval A handful of works (Chern et al., 2002; Guo et al., 2018; 2019a;b) have studied multi-source PR, defined as recovering x_1, x_2, \dots, x_L from

$$y = \left| \sum_{l=1}^L \mathbf{A}x_l \right|^2.$$

This model resembles Equation (1), but note that here the mixing occurs *before* the non-linearity. This difference makes the reconstruction problem significantly easier as it

implies the forward model is equivalent to

$$y = \left| \mathbf{A} \sum_{l=1}^L x_l \right|^2.$$

This equivalence enables the application of a standard PR algorithm to recover $\sum_{l=1}^L x_l$ followed by a standard under-determined SS algorithm to recover x_1, \dots, x_L . In contrast, the S³PR problem defined by Equation (1) does not lend itself to similar cascaded solutions as existing SS algorithms struggle to separate $|\mathbf{A}x_1|^2$ and $|\mathbf{A}x_2|^2$ when x_1 and x_2 are drawn from the same distribution/class.

Phase retrieval and blind demodulation In various imaging applications, one records measurements of a signal x_1 that is illuminated by an unknown signal x_2 . In this context, the measurement model becomes

$$y = |\mathbf{A}(x_1 \circ x_2)|^2,$$

where \circ denotes the Hadamard (elementwise) product. While solutions to this problem exist (Kane, 2008; Bendory et al., 2019), the fact that mixing occurs before the non-linearity makes the problem fundamentally different from S³PR.

2.2. Source Separation

Traditional SS algorithms assume that the sources to be separated are statistically independent and that there are as many or more observations as there are unknowns (Molgedey & Schuster, 1994; Comon, 1994; Comon & Jutten, 2010). When this is not the case, the problem is known as under-determined SS and is much more challenging.

Under-determined SS, which shows up prominently in reflection removal and hyperspectral imaging, has been accomplished by imposing priors on the reconstructed signals, for instance that they are sparse (Bofill & Zibulevsky, 2001; Li et al., 2004; Takigawa et al., 2004; Li et al., 2006; Levin & Weiss, 2007) or group sparse (Drumetz et al., 2019) in some basis. Under-determined SS can also be accomplished with convolutional neural networks (Fan et al., 2017; Zhang et al., 2018).

2.3. Inverse Problems with Deep Generative Models

Deep generative models have been used to solve a variety of under-determined imaging inverse problems.

Compressive sensing The idea of solving the compressive sensing problem by recovering the latent vectors of a deep generative model was first proposed in (Bora et al., 2017). This work has been followed up by a number of papers which have sought to improve the speed (Manoel et al., 2017; Shah & Hegde, 2018; Wu et al., 2019; Pandit

et al., 2019; Latorre et al., 2019) and generalizability (Dhar et al., 2018; Hussein et al., 2019; Asim et al., 2019) of the method.

Phase retrieval PR with generative models was introduced in (Hand et al., 2018) and (Shamshad & Ahmed, 2018). This method has since been accelerated in (Hyder et al., 2019) and applied to various PR problems in (Shamshad et al., 2019a;b).

We note in passing that optimizing the latent variables of untrained networks, following ideas proposed in (Ulyanov et al., 2018), can also be used to impose priors in order to help solve the PR problem (Jagatap & Hegde, 2019).

Other inverse problems For the sake of completeness, we note that optimizing the latent variables of a deep generative models has also been used to perform to blind demodulation (Hand & Joshi, 2019), blind deconvolution (Asim et al., 2018), and matrix decomposition (Aubin et al., 2019). We also note that optimizing the latent variables of untrained neural networks has been used for a variety of image decomposition tasks (Gandelsman et al., 2019).

3. S³PR Using Classical Algorithms

Potentially, one could solve S³PR using a sequence of classical algorithms.

3.1. SS Followed by PR

A naive solution to S³PR is to perform SS followed by PR. That is, given

$$y = \sum_{l=1}^L |\mathbf{A}x_l|^2 + w,$$

first use an under-determined SS algorithm to estimate $|\mathbf{A}x_1|^2, |\mathbf{A}x_2|^2, \dots, |\mathbf{A}x_L|^2$ and then use a PR algorithm (L times) to recover x_1, x_2, \dots, x_L from these estimates.

While conceptually straightforward, we found this idea a nonstarter. No SS algorithm we were aware of could successfully separate $|\mathbf{A}x_1|^2$ from $|\mathbf{A}x_2|^2$. The signals, illustrated for various classes of \mathbf{A} in Figure 3, were simply too unstructured and statistically similar to separate.

3.2. PR Followed by SS

While SS followed by PR failed, we found, to our surprise, that PR followed by SS worked (to a very limited degree). To understand why, note that

$$\left| \mathbf{A} \sum_{i=1}^L x_i \right|^2 = \sum_{i=1}^L |\mathbf{A}x_i|^2 + \sum_{i=1}^L \sum_{j \neq i} (\mathbf{A}x_i)^* \circ \mathbf{A}x_j, \quad (3)$$

where $(\cdot)^*$ denotes the complex conjugate of the argument.

This relationship implies that applying a PR algorithm to $\sum_{i=1}^L |\mathbf{A}x_i|^2$ is the same as applying a PR algorithm to $|\mathbf{A} \sum_{i=1}^L x_i|^2$ minus cross terms. Thus there is hope that, when the cross terms are small enough, one can recover $\sum_{i=1}^L x_i$ from $\sum_{i=1}^L |\mathbf{A}x_i|^2$.

Taking advantage of this relationship, we apply a PR algorithm followed by an under-determined SS algorithm to recover x_1, x_2, \dots, x_L . In particular, we first apply gradient descent with

$$\tilde{x} = \arg \min_x \|y - |\mathbf{A}x|^2\|_2^2, \quad (4)$$

where \tilde{x} serves as our estimate of $\sum_{l=1}^L x_l$. (We also experimented with the widely used Gerchberg-Saxton algorithm (Gerchberg, 1972) but found that it ran far slower and offered worse performance.)

We then solve the basis pursuit denoising problem from (Bofill & Zibulevsky, 2001), with a sparsifying basis, to perform SS. This results in the following optimization problem.

$$\hat{\alpha}_1, \hat{\alpha}_2, \dots, \hat{\alpha}_L = \arg \min_{\alpha_1, \alpha_2, \dots, \alpha_L} \|\tilde{x} - \sum_{i=1}^L \Psi \alpha_i\|_2^2 + \lambda \sum_i \|\alpha_i\|_1, \quad (5)$$

where λ is a tuning parameter, and Ψ denotes a sparsifying basis; we use a two dimensional inverse discrete cosine transform matrix. Our final estimates are $\hat{x}_1 = \Psi \hat{\alpha}_1, \hat{x}_2 = \Psi \hat{\alpha}_2, \dots, \hat{x}_L = \Psi \hat{\alpha}_L$.

4. S³PR Using Deep Generative Models

A better way to perform S³PR is to leverage deep generative models as priors.

Recovering latent variables We recover images x_1, x_2, \dots, x_L , with our estimates $\hat{x}_l = G(\hat{z}_l)$, from y by solving the optimization problem

$$\hat{z}_1, \hat{z}_2, \dots, \hat{z}_L = \arg \min_{z_1, z_2, \dots, z_L} \left\| y - \sum_{l=1}^L |\mathbf{A}G(z_l)|^2 \right\|_2^2, \quad (6)$$

using an alternating descent algorithm. That is, we iteratively compute the loss (6) and take a gradient step (with momentum) with respect to z_1 , then compute the loss and take a gradient step (with momentum) with respect to z_2 , etc. In practice, we found alternating descent (using the ADAM optimizer (Kingma & Ba, 2014)) provided a near monotonic reduction of the loss (see Figure 1) and ran in two minutes on an Nvidia Titan RTX GPU.

For time/resource-sensitive applications, one could also use an alternating projection algorithm (Shah & Hegde,

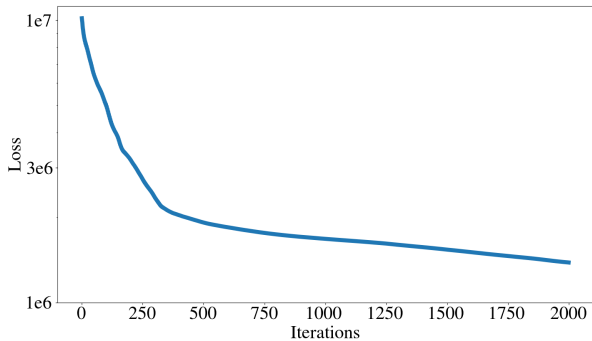


Figure 1. **Loss over Time.** Alternating descent produces a near monotonic reduction of the loss (6).

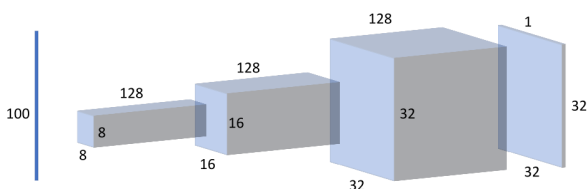


Figure 2. **Simplified DC-GAN Network Architecture.** A simple convolutional neural network, which maps a 100 dimensional latent vector to a 32×32 image, serves as our generative model.

2018; Hyder et al., 2019) or more advanced methods like AMP (Manoel et al., 2017; Pandit et al., 2019) or ADMM (Latorre et al., 2019), which can provide significantly faster convergence.

Our generative model Following (Bora et al., 2017) we use a variation of the DC-GAN (Radford et al., 2015) architecture as our deep generative model, $G(z)$. Our generator network is illustrated in Figure 2. It takes a 100 dimensional latent vector, $z \in \mathbb{R}^{100}$, as an input and applies a fully connected layer followed by a reshaping operation and batch normalization to form an $8 \times 8 \times 128$ dimensional feature map. This feature map is then upsampled $2\times$, convolved with 128 different 3×3 filters, batch normalized, and feed through a leaky ReLU to form a $16 \times 16 \times 128$ feature map. This feature map is then upsampled, convolved with 64 different 3×3 filters, batch normalized, and feed through another leaky ReLU to form a $32 \times 32 \times 64$ feature map. Finally, this feature map is convolved with a single 3×3 filter and passed through a tanh nonlinearity to form the generated image.

We train one such DC-GAN network to produce MNIST digits and another to produce Fashion MNIST articles of clothing. Each network was based off the Pytorch implementation of DC-GAN from (Linder-Norn, 2018) and was trained using the code’s default parameters. The networks were trained using the training portion of their respective

datasets and tested, as described in the next section, on a subset of the testing portion.

5. Experimental Results

We now apply two of the proposed methods to Gaussian, coded diffraction pattern (CDP), and Fourier measurements of images of numbers and articles of clothing.

We denote the PR followed by under-determined SS approach described in Section 3.2 with “PR + USS”. We call the deep generative model based approach from Section 4 “Deep S^3 PR”.

5.1. Experimental Setup

Measurement settings In each of our tests, the images have a resolution of 32×32 ($n = 1024$) and we use $4\times$ oversampling ($m = 4096$, $\mathbf{A} \in \mathbb{C}^{4096 \times 1024}$). For the case of Fourier measurements, we achieve the oversampling by first zero padding the 32×32 images to 64×64 . We apply the algorithms to mixtures of two, three, and four images. We add white Gaussian noise to all our measurements, such that they have an signal to noise ratio of 50.

We apply the algorithms to Gaussian, CDP, and Fourier measurements to generate Figures 4, 5, and 6 respectively. To generative each of the quantitative results presented in Tables 1, 2, and 3 we apply the algorithms to 10 sets of images and compute the average normalized mean-squared-error (NMSE). To account for the labeling ambiguity, that is the solution $\hat{x}_1 = A$, $\hat{x}_2 = B$ is equivalent to the solution $\hat{x}_1 = B$, $\hat{x}_2 = A$, we report the loss associated with the ordering of the solutions that produces the minimum error. There is a sign ambiguity, that is $\hat{x}_1 = A$ is an equivalent solution to $\hat{x}_1 = -A$, that we similarly account for. Likewise, for Fourier measurements, we account for the flip ambiguities of the solutions by searching, over all flips left-right and up-down, for the one that minimizes the error.

Algorithm settings Both the classical PR + USS algorithm and Deep S^3 PR method are implemented in Pytorch. Their respective optimization problems are solved with the ADAM optimizer with a learning rate of 0.02. ADAM’s momentum decay terms b_1 and b_2 are set to their default values of 0.9 and 0.999 respectively.

For PR + USS, we minimize the PR loss (4) by running the ADAM optimizer for 2000 iterations. The under-determined SS loss (5) is similarly minimized by running the ADAM optimizer for 2000 iterations. We set the tuning parameter λ to 1. (We experimented with many values of λ and found that none produced particularly accurate reconstructions.)

For Deep S^3 PR we minimize the loss (6) by running the

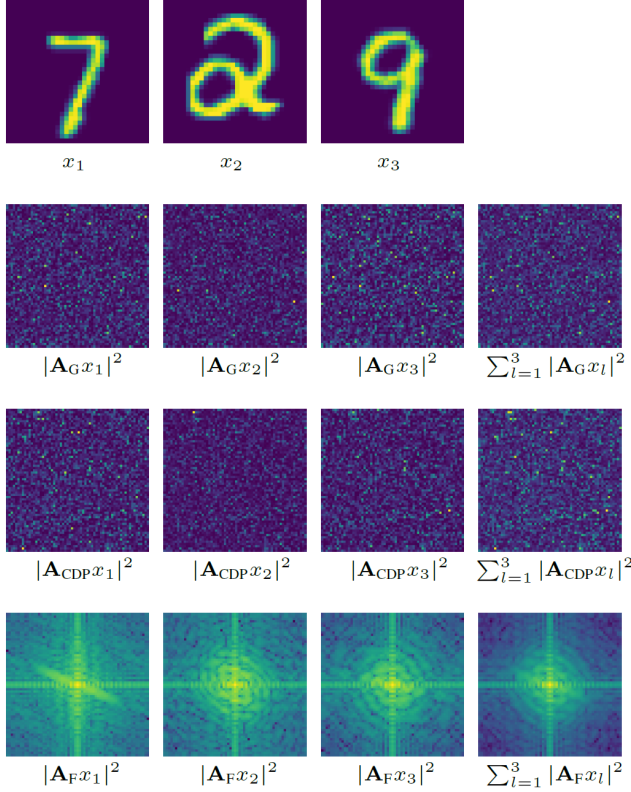


Figure 3. **Visualization of Measurements.** Examples of signals and their measurements with Gaussian (\mathbf{A}_G), CDP (\mathbf{A}_{CDP}), and Fourier (\mathbf{A}_F) measurement matrices. The Fourier measurements are displayed in log scale. The various measurements have little obvious structure. This makes separating each of them from their sum a challenging problem.

ADAM optimizer for 2 000 iterations.

For both PR + USS and Deep S³PR we perform 5 restarts. For PR + USS, at each restart the estimates \tilde{x} and $\alpha_1, \alpha_2, \dots, \alpha_L$ are initialized with random i.i.d. Gaussian vectors with mean zero and unit variance. Similarly, for Deep S³PR at each restart the latent vectors z_1, z_2, \dots, z_L are initialized with random i.i.d. Gaussian vectors with mean zero and unit variance. For both, we use the result with the smallest residual error, $\|y - \sum_l |\Psi \alpha_l|\|^2$ and $\|y - \sum_l |G(\hat{z}_l)|\|^2$ respectively, as our final solution.

Our code is available at <https://github.com/computational-imaging/DeepS3PR>.

5.2. Visualizing the Measurements

Before presenting our reconstruction results, we first present a simple visualization of the measurement we are dealing with. The top row of Figure 3 presents three example signals x_1, x_2 , and x_3 . The second row presents $|Ax_1|^2, |Ax_2|^2$, and $|Ax_3|^2$ on the left and their sum on the right, where \mathbf{A} is

a Gaussian measurement matrix. The third row presents the same for a CDP measurement matrix. The last row presents the same for a Fourier measurement matrix. The Gaussian and CDP measurements were reshaped from $64^2 \times 1$ vectors into 64×64 images for visualization.

As the figure makes clear, the measurements contain little obvious structure. This makes the task of separating each measurement from their sum extremely challenging. Existing under-determined SS algorithms are not up to the task.

5.3. Gaussian Measurements

We first test the proposed S³PR methods on complex-valued Gaussian measurement matrices. The elements of our measurement matrices are drawn from an i.i.d. circular Gaussian distribution (the real and imaginary parts of each element are drawn from i.i.d. distributions).

Results Figure 4 demonstrates that Deep S³PR is very effective with Gaussian measurement matrices. Even with mixtures of four images, Deep S³PR produces near perfect reconstructions of MNIST digits and recognizable, though imperfect, reconstructions of Fashion MNIST articles of clothing as well. In contrast, the “classical” sequential solution to S³PR completely fails with mixtures of even just two images. The quantitative results, presented in Table 1, mirror these findings.

5.4. Coded Diffraction Pattern Measurements

We next test our methods on simulated CDP measurements, which were first proposed in (Candes et al., 2015b). The CDP measurement matrix can be written as

$$\mathbf{A} = \begin{bmatrix} \mathbf{F}\mathbf{D}_1 \\ \mathbf{F}\mathbf{D}_2 \\ \vdots \\ \mathbf{F}\mathbf{D}_K \end{bmatrix}, \quad (7)$$

where \mathbf{F} represents the two dimensional Fourier transform and $\mathbf{D}_1, \mathbf{D}_2, \dots, \mathbf{D}_K$ are diagonal matrices whose diagonal entries drawn uniformly from the unit circle in the complex plane. Recall, we use a sampling rate of four: $K = 4$.

Results Figure 5 demonstrates that Deep S³PR is largely effective with CDP measurement matrices as well. With standard MNIST, Deep S³PR produces near perfect reconstructions with mixtures of up to three images, but starts to make noticeable errors with four measurements. Similarly, with Fashion MNIST, Deep S³PR largely succeeds with three images, but starts to produce minor reconstruction errors when dealing with four images. Again, the sequential solution to S³PR completely fails.

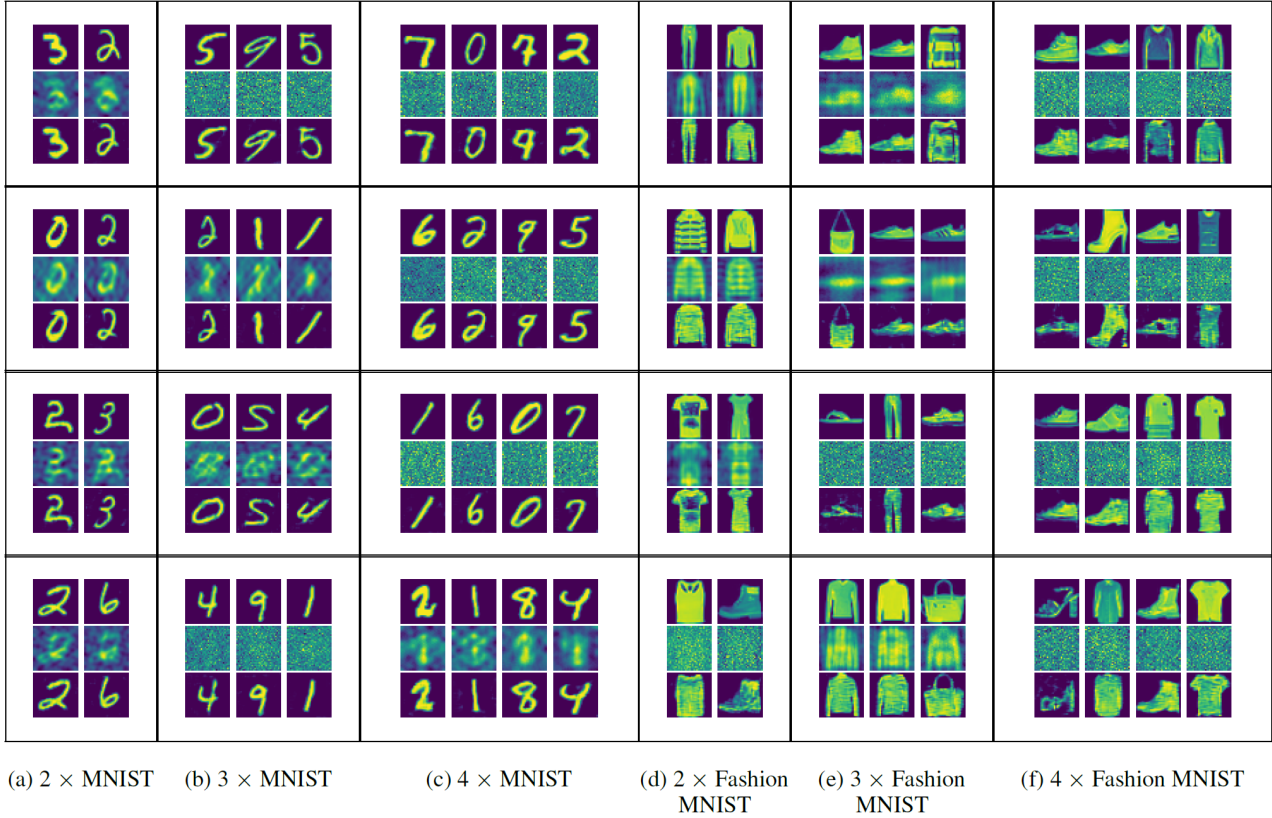


Figure 4. **Gaussian Measurement Matrix Results.** While the classical algorithm (middle row of each set) can occasionally extract some structure from the measurements, it by and large fails. In contrast, with Gaussian measurement, the proposed Deep S^3 PR technique (bottom row of each set) largely succeeds in recovering up to four mixed images. Ground truth shown in the top row of each set.

	$2 \times$ MNIST	$3 \times$ MNIST	$4 \times$ MNIST	$2 \times$ Fashion MNIST	$3 \times$ Fashion MNIST	$4 \times$ Fashion MNIST
PR + USS	$.27 \pm .02$	$.85 \pm .34$	$.91 \pm .30$	$.39 \pm .24$	$.70 \pm .34$	$1.06 \pm .10$
Deep S^3 PR	$.01 \pm .01$	$.02 \pm .01$	$.05 \pm .03$	$.08 \pm .05$	$.13 \pm .11$	$0.15 \pm .04$

Table 1. Average NMSE across 10 sets of test images with Gaussian measurement matrices.

5.5. Fourier Measurements

Finally, we test the proposed methods with Fourier measurements, which is arguably their most important use case. Fourier measurements form the basis of most coherence diffraction imaging systems (Miao et al., 1999) as well as various correlation-based imaging systems (Bertolotti et al., 2012; Katz et al., 2014; Metzler et al., 2020).

Preconditioning. When dealing with Fourier measurements, we precondition the reconstruction problem by solving

$$\arg \min_{z_1, z_2, \dots, z_L} \|\mathbf{F}^{-1}y - \mathbf{F}^{-1} \sum_{l=1}^L |\mathbf{F}G(z_l)|^2\|_2^2. \quad (8)$$

which, through the relationship $\mathbf{F}(x \star x) = |\mathbf{F}x|^2$, is equivalent to

$$\arg \min_{z_1, z_2, \dots, z_L} \|\mathbf{F}^{-1}y - \sum_{l=1}^L G(z_l) \star G(z_l)\|_2^2. \quad (9)$$

We have found the latter formulation offers noticeably better performance.

Results Fourier measurements prove to be significantly more challenging than Gaussian or CDP measurements. Figure 6 demonstrates that with even just three MNIST images, Deep S^3 PR starts to make significant errors. While the technique can often reconstruct the general shape of Fashion MNIST images, there are significant artifacts in most of the reconstructions. Table 3 shows these errors show up in the average NMSE as well.

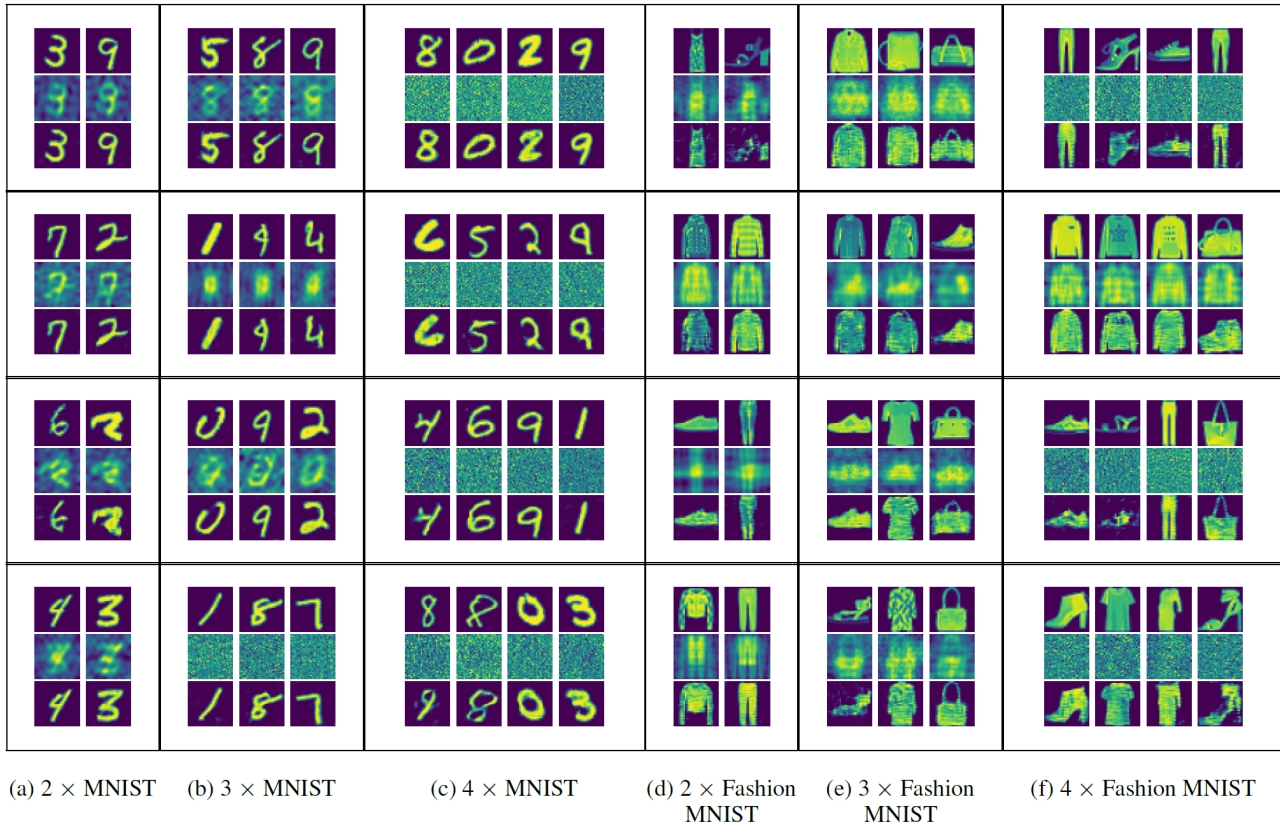


Figure 5. **Coded Diffraction Pattern Measurement Matrix Results.** With CDP measurements the classical algorithm (middle row of each set) begins to fail with just two images. In contrast the proposed Deep S³PR method (bottom row of each set) again succeeds in recovering up to four mixed images. Ground truth shown in the top row of each set.

	$2 \times$ MNIST	$3 \times$ MNIST	$4 \times$ MNIST	$2 \times$ Fashion MNIST	$3 \times$ Fashion MNIST	$4 \times$ Fashion MNIST
PR + USS	$.27 \pm .03$	$.88 \pm .34$	$1.08 \pm .12$	$.38 \pm .09$	$.44 \pm .09$	$.90 \pm .22$
Deep S ³ PR	$.01 \pm .01$	$.02 \pm .02$	$0.04 \pm .02$	$.06 \pm .03$	$.14 \pm .06$	$.14 \pm .09$

Table 2. Average NMSE across 10 sets of test images with CDP measurement matrices.

With Fourier measurements the sequential PR + USS algorithm fails with even two images.

6. Discussion

This work introduces the S³PR problem and develops a deep generative model based solution to it. We demonstrate that our proposed Deep S³PR solution can solve S³PR with multiple images across a variety of different measurement matrices. Accordingly, this work stands to enable new optical capabilities, such as imaging extended objects through scattering media (Bertolotti et al., 2012; Katz et al., 2014) or around corners (Metzler et al., 2020). It also opens up a number of new research directions for the ML community.

References

- Asim, M., Shamshad, F., and Ahmed, A. Blind image deconvolution using deep generative priors. *arXiv preprint arXiv:1802.04073*, 2018.
- Asim, M., Ahmed, A., and Hand, P. Invertible generative models for inverse problems: mitigating representation error and dataset bias. *arXiv preprint arXiv:1905.11672*, 2019.
- Aubin, B., Loureiro, B., Maillard, A., Krzakala, F., and Zdeborová, L. The spiked matrix model with generative priors. In *Advances in Neural Information Processing Systems*, pp. 8364–8375, 2019.
- Bahmani, S. and Romberg, J. Phase retrieval meets statis-

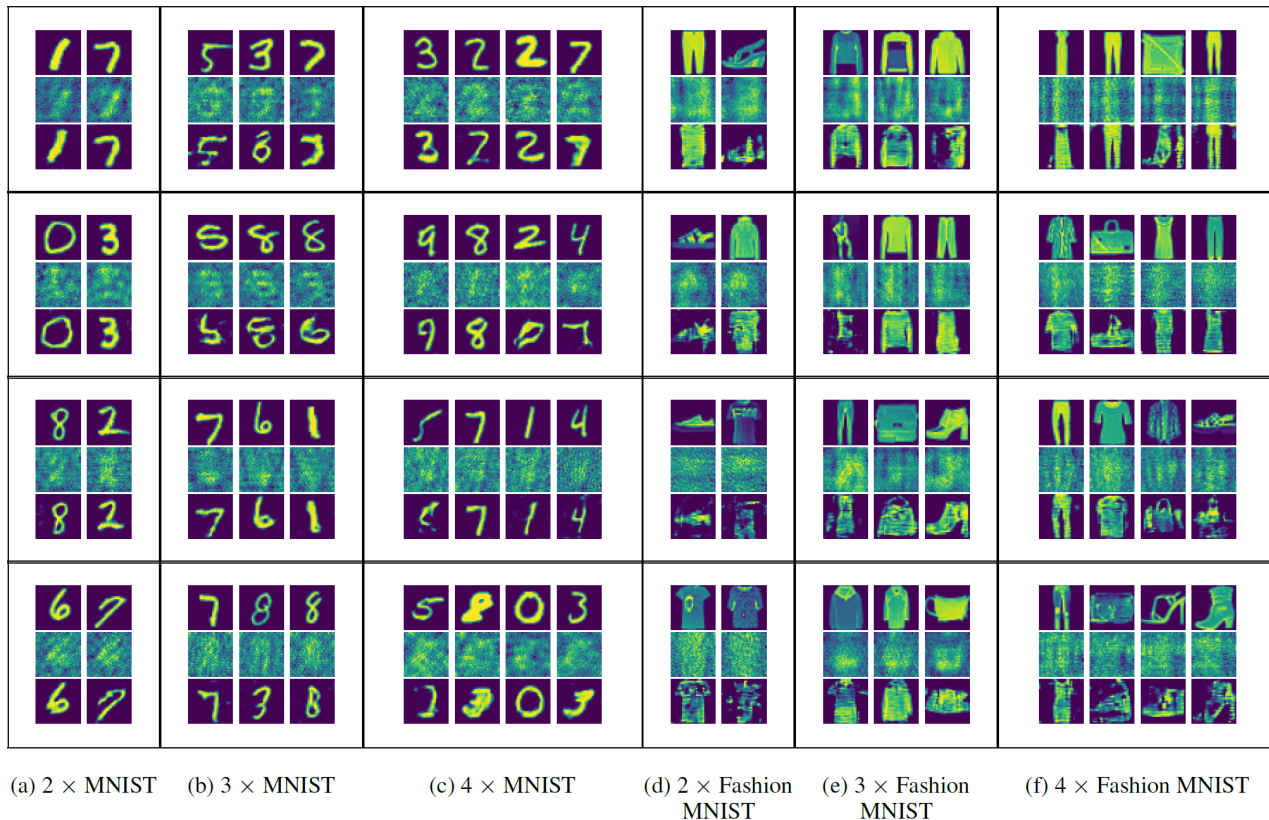


Figure 6. Fourier Measurement Matrix Results. Fourier measurements are particularly challenging. While the classical algorithm (middle row of each set) is again unable to reconstruct the images, the proposed Deep S^3 PR method (bottom row of each set) recovers sets of two images but starts to make significant errors when tasked with recovering three or more images. With Fashion MNIST, noticeable reconstruction artifacts appear with just two images. Ground truth shown in the top row of each set.

	2 × MNIST	3 × MNIST	4 × MNIST	2 × Fashion MNIST	3 × Fashion MNIST	4 × Fashion MNIST
PR + USS	.47 ± .05	.54 ± .03	.61 ± .02	.48 ± .09	.61 ± .07	.64 ± .07
Proposed	.11 ± .06	.21 ± .10	.21 ± .06	.25 ± .07	.38 ± .12	.41 ± .14

Table 3. Average NMSE across 10 sets of test images with Fourier measurement matrices.

- tical learning theory: A flexible convex relaxation. In *Artificial Intelligence and Statistics*, pp. 252–260, 2017.
- Bendory, T., Edidin, D., and Eldar, Y. C. Blind phaseless short-time fourier transform recovery. *IEEE Transactions on Information Theory*, 2019.
- Bertolotti, J., Van Putten, E. G., Blum, C., Lagendijk, A., Vos, W. L., and Mosk, A. P. Non-invasive imaging through opaque scattering layers. *Nature*, 491(7423): 232–234, 2012.
- Bofill, P. and Zibulevsky, M. Underdetermined blind source separation using sparse representations. *Signal processing*, 81(11):2353–2362, 2001.
- Bora, A., Jalal, A., Price, E., and Dimakis, A. G. Compressed sensing using generative models. In *Proceedings of the 34th International Conference on Machine Learning-Volume 70*, pp. 537–546. JMLR. org, 2017.
- Candes, E., Strohmer, T., and Voroninski, V. Phaselift: Exact and stable signal recovery from magnitude measurements via convex programming. *Communications on Pure and Applied Mathematics*, 66(8):1241–1274, 2013.
- Candes, E., Li, X., and Soltanolkotabi, M. Phase retrieval via wirtinger flow: Theory and algorithms. *IEEE Transactions on Information Theory*, 61(4):1985–2007, 2015a.
- Candes, E., Li, X., and Soltanolkotabi, M. Phase retrieval

- from coded diffraction patterns. *Applied and Computational Harmonic Analysis*, 39(2):277–299, 2015b.
- Chandra, R., Studer, C., and Goldstein, T. Phasepack: A phase retrieval library. *arXiv preprint arXiv:1711.10175*, 2017.
- Chern, J.-L., Li, C.-C., and Tseng, S.-H. Blind phase retrieval and source separation of electromagnetic fields. *Optics letters*, 27(2):89–91, 2002.
- Comon, P. Independent component analysis, a new concept? *Signal processing*, 36(3):287–314, 1994.
- Comon, P. and Jutten, C. *Handbook of Blind Source Separation: Independent component analysis and applications*. Academic press, 2010.
- Dhar, M., Grover, A., and Ermon, S. Modeling sparse deviations for compressed sensing using generative models. *arXiv preprint arXiv:1807.01442*, 2018.
- Drumetz, L., Meyer, T. R., Chanussot, J., Bertozzi, A. L., and Jutten, C. Hyperspectral image unmixing with endmember bundles and group sparsity inducing mixed norms. *IEEE Transactions on Image Processing*, 28(7):3435–3450, 2019.
- Fan, Q., Yang, J., Hua, G., Chen, B., and Wipf, D. A generic deep architecture for single image reflection removal and image smoothing. In *Proceedings of the IEEE International Conference on Computer Vision*, pp. 3238–3247, 2017.
- Fienup, J. Reconstruction of an object from the modulus of its fourier transform. *Optics letters*, 3(1):27–29, 1978.
- Fienup, J. Phase retrieval algorithms: a comparison. *Applied optics*, 21(15):2758–2769, 1982.
- Gandelsman, Y., Shocher, A., and Irani, M. "double-dip": Unsupervised image decomposition via coupled deep-image-priors. In *The IEEE Conference on Computer Vision and Pattern Recognition (CVPR)*, June 2019.
- Gerchberg, R. A practical algorithm for the determination of phase from image and diffraction plane pictures. *Optik*, 35:237, 1972.
- Goldstein, T. and Studer, C. Phasemax: Convex phase retrieval via basis pursuit. *arXiv preprint arXiv:1610.07531*, 2016.
- Griffin, D. and Lim, J. Signal estimation from modified short-time fourier transform. *Acoustics, Speech and Signal Processing, IEEE Transactions on*, 32(2):236–243, 1984.
- Guo, Y., Wang, A., and Wang, W. Multi-source phase retrieval from multi-channel phaseless stft measurements. *Signal Processing*, 144:36–40, 2018.
- Guo, Y., Wang, T., Li, J., Wang, A., and Wang, W. Multiple input single output phase retrieval. *Circuits, Systems, and Signal Processing*, pp. 1–23, 2019a.
- Guo, Y., Zhao, X., Li, J., Wang, A., and Wang, W. Blind multiple input multiple output image phase retrieval. *IEEE Transactions on Industrial Electronics*, 2019b.
- Hand, P. and Joshi, B. Global guarantees for blind demodulation with generative priors. *arXiv preprint arXiv:1905.12576*, 2019.
- Hand, P., Leong, O., and Voroninski, V. Phase retrieval under a generative prior. In *Advances in Neural Information Processing Systems*, pp. 9136–9146, 2018.
- Hassanieh, H., Abari, O., Rodriguez, M., Abdelghany, M., Katabi, D., and Indyk, P. Fast millimeter wave beam alignment. In *Proceedings of the 2018 Conference of the ACM Special Interest Group on Data Communication*, pp. 432–445. ACM, 2018.
- Hussein, S. A., Tirer, T., and Giryes, R. Image-adaptive gan based reconstruction. *arXiv preprint arXiv:1906.05284*, 2019.
- Hyder, R., Shah, V., Hegde, C., and Asif, M. S. Alternating phase projected gradient descent with generative priors for solving compressive phase retrieval. In *ICASSP 2019-2019 IEEE International Conference on Acoustics, Speech and Signal Processing (ICASSP)*, pp. 7705–7709. IEEE, 2019.
- Jagatap, G. and Hegde, C. Phase retrieval using untrained neural network priors. In *NeurIPS 2019 Workshop on Solving Inverse Problems with Deep Networks*, 2019.
- Kane, D. J. Principal components generalized projections: a review. *JOSA B*, 25(6):A120–A132, 2008.
- Katz, O., Heidmann, P., Fink, M., and Gigan, S. Non-invasive single-shot imaging through scattering layers and around corners via speckle correlations. *Nature photonics*, 8(10):784, 2014.
- Kingma, D. P. and Ba, J. Adam: A method for stochastic optimization. *arXiv preprint arXiv:1412.6980*, 2014.
- Latorre, F., Cevher, V., et al. Fast and provable adm for learning with generative priors. In *Advances in Neural Information Processing Systems*, pp. 12004–12016, 2019.
- Levin, A. and Weiss, Y. User assisted separation of reflections from a single image using a sparsity prior. *IEEE Transactions on Pattern Analysis and Machine Intelligence*, 29(9):1647–1654, 2007.

- Li, Y., Cichocki, A., and Amari, S.-i. Analysis of sparse representation and blind source separation. *Neural computation*, 16(6):1193–1234, 2004.
- Li, Y., Amari, S.-I., Cichocki, A., Ho, D. W., and Xie, S. Underdetermined blind source separation based on sparse representation. *IEEE Transactions on signal processing*, 54(2):423–437, 2006.
- Linder-Norn, E. Pytorch generative adversarial networks. <https://github.com/eriklindernoren/PyTorch-GAN>, 2018. Accessed: 2020-1-14.
- Liu, Z., Luo, P., Wang, X., and Tang, X. Deep learning face attributes in the wild. In *Proceedings of International Conference on Computer Vision (ICCV)*, December 2015.
- Manoel, A., Krzakala, F., Mézard, M., and Zdeborová, L. Multi-layer generalized linear estimation. In *2017 IEEE International Symposium on Information Theory (ISIT)*, pp. 2098–2102. IEEE, 2017.
- Metzler, C., Maleki, A., and Baraniuk, R. BM3D-PRGAMP: Compressive phase retrieval based on BM3D denoising. In *2016 IEEE International Conference on Image Processing (ICIP)*, pp. 2504–2508. IEEE, 2016.
- Metzler, C. A., Heide, F., Rangarajan, P., Balaji, M. M., Viswanath, A., Veeraraghavan, A., and Baraniuk, R. G. Deep-inverse correlography: towards real-time high-resolution non-line-of-sight imaging. *Optica*, 7(1): 63–71, Jan 2020. doi: 10.1364/OPTICA.374026. URL <http://www.osapublishing.org/optica/abstract.cfm?URI=optica-7-1-63>.
- Miao, J., Charalambous, P., Kirz, J., and Sayre, D. Extending the methodology of x-ray crystallography to allow imaging of micrometre-sized non-crystalline specimens. *Nature*, 400(6742):342, 1999.
- Molgedey, L. and Schuster, H. G. Separation of a mixture of independent signals using time delayed correlations. *Physical review letters*, 72(23):3634, 1994.
- Moravec, M. L., Romberg, J. K., and Baraniuk, R. G. Compressive phase retrieval. In *Optical Engineering+ Applications*, pp. 670120–670120. International Society for Optics and Photonics, 2007.
- Mukherjee, S. and Seelamantula, C. S. An iterative algorithm for phase retrieval with sparsity constraints: application to frequency domain optical coherence tomography. In *2012 IEEE International Conference on Acoustics, Speech and Signal Processing (ICASSP)*, pp. 553–556. IEEE, 2012.
- Pandit, P., Sahraee-Ardakan, M., Rangan, S., Schniter, P., and Fletcher, A. K. Inference with deep generative priors in high dimensions. *arXiv preprint arXiv:1911.03409*, 2019.
- Pfeifer, M., Williams, G., Vartanyants, I., Harder, R., and Robinson, I. Three-dimensional mapping of a deformation field inside a nanocrystal. *Nature*, 442(7098):63–66, 2006.
- Radford, A., Metz, L., and Chintala, S. Unsupervised representation learning with deep convolutional generative adversarial networks. *arXiv preprint arXiv:1511.06434*, 2015.
- Rajaei, B., Tramel, E. W., Gigan, S., Krzakala, F., and Daudet, L. Intensity-only optical compressive imaging using a multiply scattering material and a double phase retrieval approach. In *2016 IEEE International Conference on Acoustics, Speech and Signal Processing (ICASSP)*, pp. 4054–4058. IEEE, 2016.
- Rodriguez, J., Xu, R., Chen, C., Zou, Y., and Miao, J. Oversampling smoothness: an effective algorithm for phase retrieval of noisy diffraction intensities. *Journal of applied crystallography*, 46(2):312–318, 2013.
- Schniter, P. and Rangan, S. Compressive phase retrieval via generalized approximate message passing. *IEEE Transactions on Signal Processing*, 63(4):1043–1055, 2015.
- Shah, V. and Hegde, C. Solving linear inverse problems using gan priors: An algorithm with provable guarantees. In *2018 IEEE International Conference on Acoustics, Speech and Signal Processing (ICASSP)*, pp. 4609–4613. IEEE, 2018.
- Shamshad, F. and Ahmed, A. Robust compressive phase retrieval via deep generative priors. *arXiv preprint arXiv:1808.05854*, 2018.
- Shamshad, F., Abbas, F., and Ahmed, A. Deep ptych: Subsampled fourier ptychography using generative priors. In *ICASSP 2019-2019 IEEE International Conference on Acoustics, Speech and Signal Processing (ICASSP)*, pp. 7720–7724. IEEE, 2019a.
- Shamshad, F., Hanif, A., Abbas, F., Awais, M., and Ahmed, A. Adaptive ptych: Leveraging image adaptive generative priors for subsampled fourier ptychography. In *Proceedings of the IEEE International Conference on Computer Vision Workshops*, pp. 0–0, 2019b.
- Sharma, M., Metzler, C. A., Nagesh, S., Cossairt, O., Baraniuk, R. G., and Veeraraghavan, A. Inverse scattering via transmission matrices: Broadband illumination and fast phase retrieval algorithms. *IEEE Transactions on Computational Imaging*, 2019.

- Takigawa, I., Kudo, M., and Toyama, J. Performance analysis of minimum ℓ_1 -norm solutions for underdetermined source separation. *IEEE transactions on signal processing*, 52(3):582–591, 2004.
- Tillmann, A., Eldar, Y., and Mairal, J. Dolphin-dictionary learning for phase retrieval. *IEEE Transactions on Signal Processing*, 64(24):6485–6500, 2016.
- Ulyanov, D., Vedaldi, A., and Lempitsky, V. Deep image prior. In *Proceedings of the IEEE Conference on Computer Vision and Pattern Recognition*, pp. 9446–9454, 2018.
- Wu, Y., Rosca, M., and Lillicrap, T. Deep compressed sensing. In *International Conference on Machine Learning*, pp. 6850–6860, 2019.
- Xiao, H., Rasul, K., and Vollgraf, R. Fashion-mnist: a novel image dataset for benchmarking machine learning algorithms. *arXiv preprint arXiv:1708.07747*, 2017.
- Zhang, X., Ng, R., and Chen, Q. Single image reflection separation with perceptual losses. In *Proceedings of the IEEE Conference on Computer Vision and Pattern Recognition*, pp. 4786–4794, 2018.